

BIOPHYSICS

The mechanism of gap creation by a multifunctional nuclease during base excision repair

Jungmin Yoo^{1,2,3†}, Donghun Lee^{1,2,3†}, Hyeryeon Im^{1,2†}, Sangmi Ji^{1,2}, Sanghoon Oh^{2,4}, Minsang Shin⁵, Daeho Park^{1,3}, Gwangrog Lee^{1,2,3,4*}

During base excision repair, a transient single-stranded DNA (ssDNA) gap is produced at the apurinic/aprimidinic (AP) site. Exonuclease III, capable of performing both AP endonuclease and exonuclease activity, are responsible for gap creation in bacteria. We used single-molecule fluorescence resonance energy transfer to examine the mechanism of gap creation. We found an AP site anchor-based mechanism by which the intrinsically distributive enzyme binds strongly to the AP site and becomes a processive enzyme, rapidly creating a gap and an associated transient ssDNA loop. The gap size is determined by the rigidity of the ssDNA loop and the duplex stability of the DNA and is limited to a few nucleotides to maintain genomic stability. When the 3' end is released from the AP endonuclease, polymerase I quickly initiates DNA synthesis and fills the gap. Our work provides previously unidentified insights into how a signal of DNA damage changes the enzymatic functions.

INTRODUCTION

Every day, DNA is damaged by the natural by-products of cellular metabolism (e.g., oxygen radicals and chemical species) and ionizing radiation (e.g., ultraviolet, α , β , and γ rays) (1). Failing to repair the damage results in the accumulation of genotoxic intermediates and cytotoxic mutagens, leading to cell death and cancer in humans. However, all organisms have evolved sophisticated mechanisms to efficiently repair DNA lesions. Base damage, the most common DNA lesion, is caused by alkylation, oxidation, deamination, and depurination/depyrimidination (1). The chemical modification of DNA bases affects the primary structure of the DNA duplex. A series of enzymes recognize and process various kinds of DNA base damage in sequence in a process called base excision repair (BER).

BER plays a central role in maintaining genomic integrity (2) and in the epigenetic demethylation of the genome (3). The enzymes involved in BER, which are conserved from bacteria to humans, work in concert to restore damaged bases. First, all damaged bases are cleaved and converted into apurinic/aprimidinic (AP) sites by damage-specific glycosylases. The resulting AP sites are a prominent feature because of the missing base. They are recognized and processed by a series of enzymatic reactions that consists of five key enzymatic steps (4): (i) excision of the damaged base by a glycosylase; (ii) cutting (incision) of the phosphodiester backbone by an AP endonuclease; (iii) gap creation by an exonuclease; (iv) gap filling by a polymerase, which restores the excised nucleotides and removes the DNA backbone without nucleobases; and (v) sealing of the nick by a ligase.

Upon the removal of the damaged bases by glycosylases, the two main families of AP endonucleases, exonuclease III (ExoIII) and endonuclease IV, precisely cut the phosphodiester backbone of DNA. ExoIII in *Escherichia coli* and apurinic/aprimidinic endonuclease I and II (APE1 and APE2) in humans are ExoIII family members and the main AP endonucleases responsible for processing over 80% of base damage (5, 6). ExoIII is a multifunctional enzyme that functions as both an AP endonuclease and an exonuclease (7, 8). In the absence of AP sites, it degrades the 3' end of double-stranded DNA (dsDNA) in the 3'-to-5' direction, releasing 5' mononucleotides and producing a stretch of single-stranded DNA (ssDNA) on the opposite strand (9, 10). At AP sites, in contrast, it cuts the phosphodiester bond on the 5' side of the site using its endonuclease function and removes 3' terminal groups on the hydrolyzable strand of dsDNA. This action creates a small ssDNA gap from the AP site by excising the minimal amount of DNA needed for efficient repair.

It remains unknown how both enzymatic activities are coordinated during gap creation and how the gap size is limited to a few nucleotides for optimal repair. The gap as an essential intermediate recruits polymerase to prime the next step of DNA synthesis in BER (11), and the control of gap size is particularly important for the efficiency of DNA repair: If the gap is too large, then it becomes a target for ssDNA-specific nucleases; if the gap is too small, then DNA polymerase cannot bind the DNA to initiate DNA synthesis. In addition, uncontrolled exonuclease activity would degrade a notable amount of DNA, jeopardizing genome stability. However, despite its importance, the mechanism of gap creation remains to be elucidated.

Information on protein dynamics is essential to relate the enzyme-substrate interaction to enzyme function (12–14). Furthermore, such information provides an opportunity to unravel the underlying mechanism that drives catalysis on a relevant time scale. Despite the available structural information about ExoIII and the biochemical studies on the five steps of BER performed to date, the molecular basis of gap creation and aspects of spatiotemporal function control that delicately maintain genome stability has not been determined owing to the lack of real-time dynamics information. Recent progress in single-molecule detection has provided unprecedented resolution for studying the mechanisms of enzymes

Copyright © 2021
The Authors, some
rights reserved;
exclusive licensee
American Association
for the Advancement
of Science. No claim to
original U.S. Government
Works. Distributed
under a Creative
Commons Attribution
NonCommercial
License 4.0 (CC BY-NC).

Downloaded from https://www.science.org at Gwangju Institute of Science and Technology on September 06, 2024

¹School of Life Sciences, Gwangju Institute of Science and Technology, Gwangju 61005, Korea. ²Single-Molecule Biology Laboratory, Gwangju Institute of Science and Technology, Gwangju 61005, Korea. ³Cell Mechanobiology Laboratory, Gwangju Institute of Science and Technology, Gwangju 61005, Korea. ⁴Department of Biomedical Science and Engineering, Gwangju Institute of Science and Technology, Gwangju 61005, Korea. ⁵Department of Microbiology, School of Medicine, Kyungpook National University, 680 Gukchaebosang-Ro, Jung-gu, Daegu 41944, Korea.

*Corresponding author. Email: glee@gist.ac.kr

†These authors contributed equally to this work.

(15–17), the correlation between structural dynamics and function (18, 19), and the dynamic intermediates of many biological molecules (20, 21).

In this study, we used single-molecule fluorescence resonance energy transfer (smFRET) to address how the dual function of ExoIII is regulated on different substrates and in different buffer conditions. We found that, in the absence of an AP site (i.e., at abasic sites), ExoIII distributively converts dsDNA to ssDNA, whereas in the presence of an AP site, it specifically cleaves dsDNA at the AP site and then processively degrades a limited number of nucleotides (nt). Gap creation relies on both the strong affinity of ExoIII to the AP site, achieved by stacking a tryptophan (Trp²¹²) indole ring on the AP site nucleotide sugar ribose ring, and on the physiological salt conditions, which determine the rigidity of ssDNA and the stability of dsDNA.

RESULTS

ExoIII folds into a four-layered globular protein that is organized into a twofold symmetric topology: The two inside layers are composed of six-stranded β sheets, and the two outside layers are flanked by two parallel sets of α helices (Fig. 1A) (22). ExoIII family members in higher organisms have adopted the catalytic core domains of the bacterial enzyme within their overall structural framework. ExoIII in bacteria and the homolog APE1 in humans are the main 5' AP endonucleases in their respective BER pathways. From the ExoIII enzyme structure, it was postulated that ExoIII binds DNA using its α_M helix (Fig. 1B, blue) to hold the 3' end of the undamaged DNA backbone via the DNA major groove (22). It has been hypothesized that the base stacking between Trp²¹² and the sugar ring at the AP site ensures the specificity of cleavage (22, 23). The active site is located at the center of the groove between the two β sheets (Fig. 1B, green). Polar residues within the active site form a hydrogen bonding network with a number of ordered water molecules, allowing a carboxylate in Asp¹⁵¹ to alter its pK_a to protonate the O3' leaving group, thus facilitating a nucleophilic attack on the P–O3' bond during the cleavage reaction (22).

To monitor exonuclease activity at the single-molecule level, we constructed a blunt-ended dsDNA substrate in which the fluorescent donor (Cy3) is attached to the 5' end of the unhydrolyzed strand, and the acceptor (Cy5) is 20 bp away from the 5' end on the same strand (Fig. 1C, left). The DNA was immobilized on a polymer-coated quartz surface via biotin-streptavidin interactions (24). When a reaction solution containing ExoIII and 10 mM MgCl₂ was introduced with a flow channel system (25) to the surface-tethered DNA molecules, the 3' strand was degraded by ExoIII, and the resulting 5' single strand coiled up (Fig. 1C). In this work, we refer to this type of experiment as a “multiturnover reaction” because multiple binding and dissociation events could be performed during degradation by free proteins capable of rebinding the substrate.

Figure 1D displays a typical individual FRET time trajectory obtained from single DNA molecules degraded by ExoIII. The abrupt increases in fluorescence in the donor due to the protein-induced enhancement of fluorescence reveal the moment of protein binding (26–28). We measured the degradation time, marked by the green region, during which FRET efficiency rises from its minimum to its maximum (Fig. 1D). Such an increase was not observed in the absence of Mg²⁺ (fig. S1, A and B) and was attributed to degradation of the 3' end from the blunt-ended dsDNA as shown in the gel assay

under the same reaction condition (fig. S1C). The change in the FRET signal thus reports on the progress of degradation in real time, as demonstrated in a previous study (13). The peak around $E = 0$ came from the donor-only DNA species, comprising molecules with inactive acceptors (Fig. 1E). Although that population does not report on degradation, it provides a reference for $E = 0$. Before the reaction, the histogram peaked at $E = 0.19$, whereas after the reaction, it peaked at $E = 0.76$. To determine whether the $E = 0.76$ state originated from the degradation product, we made an ssDNA construct that mimicked the reaction product (right cartoon in Fig. 1C) and obtained the same FRET peak at $E = 0.76$ (Fig. 1F).

To quantify a type of nuclease, the degradation periods of the blunt-ended DNA were dissected and analyzed as a function of the concentration of ExoIII ([ExoIII]). The degradation periods became shorter with increasing [ExoIII] (fig. S2), and this concentration-dependent enzymatic reaction was classified as a distributive manner (13), where the degradation time becomes longer if the enzyme tends to dissociate because the degradation reaction halts until the enzyme rebinds to the DNA substrate at low concentrations.

To monitor the activity of AP endonuclease at the AP site, we extended the original blunt substrate by 5 nt on the 3' end of the hydrolyzed strand because ssDNA is resistant to degradation by ExoIII, and a 3' overhang of 4 nt or longer can prevent the initiation of exonuclease activity (9). We introduced an AP site between the two fluorophores (top in Fig. 2A) and named this substrate “AP-DNA.” In the presence of Mg²⁺, ExoIII cuts the DNA backbone at the AP site via its AP endonuclease activity and subsequently generates an ssDNA gap via its exonuclease activity (11, 29, 30), whereas in the presence of Ca²⁺, it acts as only an AP endonuclease and nicks the AP site without significant degradation (fig. S3) (31). If Ca²⁺ is exchanged with Mg²⁺ in the flow cell, the enzyme also resumes degradation at a nick.

The FRET value of this construct (AP-DNA) was ~ 0.27 before the reaction (Fig. 2A, black peak in the middle panel) and ~ 0.63 after the reaction (Fig. 2A, red peak in the middle panel). We made a DNA construct that mimicked the reaction product and obtained the same FRET peak at $E = \sim 0.63$ (fig. S4, A and B). In contrast, no significant degradation was observed for the 3' end extended control substrate without an AP site (fig. S4C), suggesting that the FRET change came from AP site-specific degradation. The consistency between smFRET results and gel assays (Fig. 2, H and I) indicated that smFRET is a sensitive assay for studying the dynamics of DNA degradation in real time, particularly for the processing of the gap in AP-DNA, which is a critical intermediate step during BER.

To investigate the effect of AP sites on enzymatic activity, we compared the degradation of AP-DNA and blunt-ended DNA under the same conditions (Fig. 2, A and B). At 5 nM [ExoIII], the representative trace (Fig. 2A, bottom) obtained from the AP-DNA showed a rapid increase in FRET with an average degradation time of 1.60 ± 0.08 s/nt (SEM, $n = 84$), whereas the trace (Fig. 2B, bottom) obtained from the blunt-ended DNA displayed a much slower progression, with an average degradation time of 8.06 ± 0.55 s/nt (SEM, $n = 70$). The approximately fivefold difference (Fig. 2E) indicates that the exonucleolytic activity somehow becomes processive in the presence of AP sites.

In an attempt to test whether the AP site was indeed the origin of the processive degradation, we constructed two nicked substrates in the same configuration but with and without an AP site between the

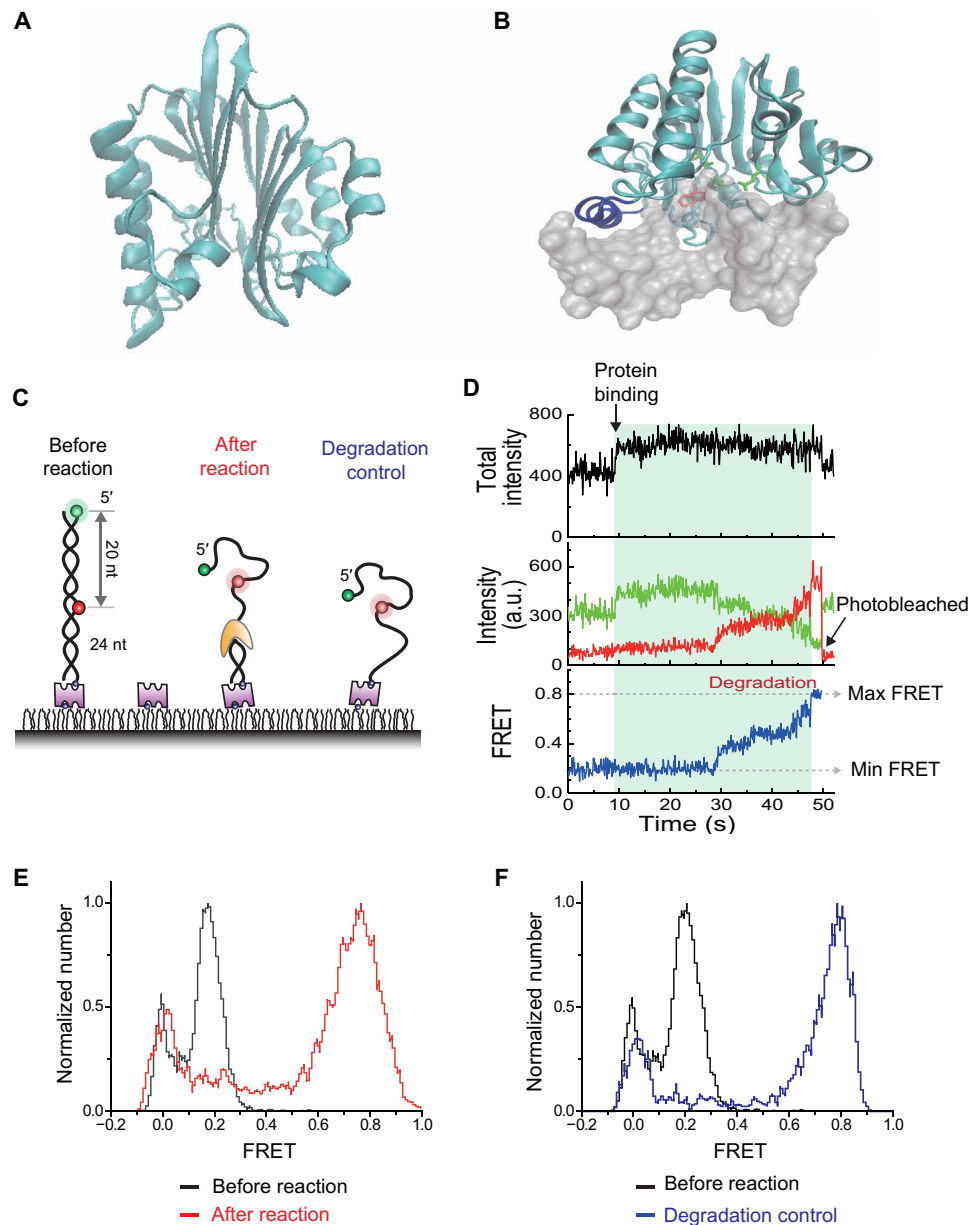


Fig. 1. Structure of ExoIII and smFRET assay. (A) Twofold symmetric topology of ExoIII (PDB entry: 1AKO). (B) Modeled DNA-enzyme complex reconstituted in silico from ExoIII (PDB entry: 1AKO) and DNA (PDB entry: 1DE8), showing the active site (green), the binding of the protruding α helix into the DNA major groove (blue), and AP site-specific binding (red). (C) Experimental schematics before (left) and after (middle) degradation by ExoIII and an ssDNA mimicking the degradation product (right). ExoIII converts the dsDNA between the donor (green) and the acceptor (red) to ssDNA, resulting in an increase in FRET efficiency. (D) A representative FRET time trajectory under 80 nM ExoIII and 10 mM Mg^{2+} , showing how the degradation time is measured. The total intensity is the sum of the donor and acceptor intensities (black, top). Green and red curves represent the donor and acceptor intensities, respectively (middle), and the blue curve represents the calculated FRET efficiency (bottom). a.u., arbitrary units. (E) smFRET histograms before (black) and after a 2-min reaction (red). (F) smFRET histograms of dsDNA (black) and ssDNA (blue) as degradation products in the absence of ExoIII.

donor and acceptor dyes (Fig. 2, C and D). The nicked substrate without the AP site (termed nicked DNA) exhibited much slower degradation on the FRET time trace, whereas the nicked substrate with the AP site (termed nicked AP-DNA) had a rapid increase in FRET efficiency, reconfirming that ExoIII became more processive in the presence of the AP site (exemplary traces in Fig. 2, C and D). The degradation time of the nicked AP-DNA was ~ 3 times shorter than that for the nicked DNA at the same [ExoIII] of 5 nM (Fig. 2E).

We conjectured that the enzyme tightly bound the AP site, performing processive degradation without dissociating from the substrate.

To assess the degradation rates of different types of DNA substrates, the inverse of characteristic times (τ_1) was plotted as a function of [ExoIII] after the 2-min reaction (Fig. 2F and fig. S5). The substrate with the AP site was degraded much faster than other substrates. ExoIII has been reported to have a strong salt dependence (31). To test whether the difference in degradation rates resulted

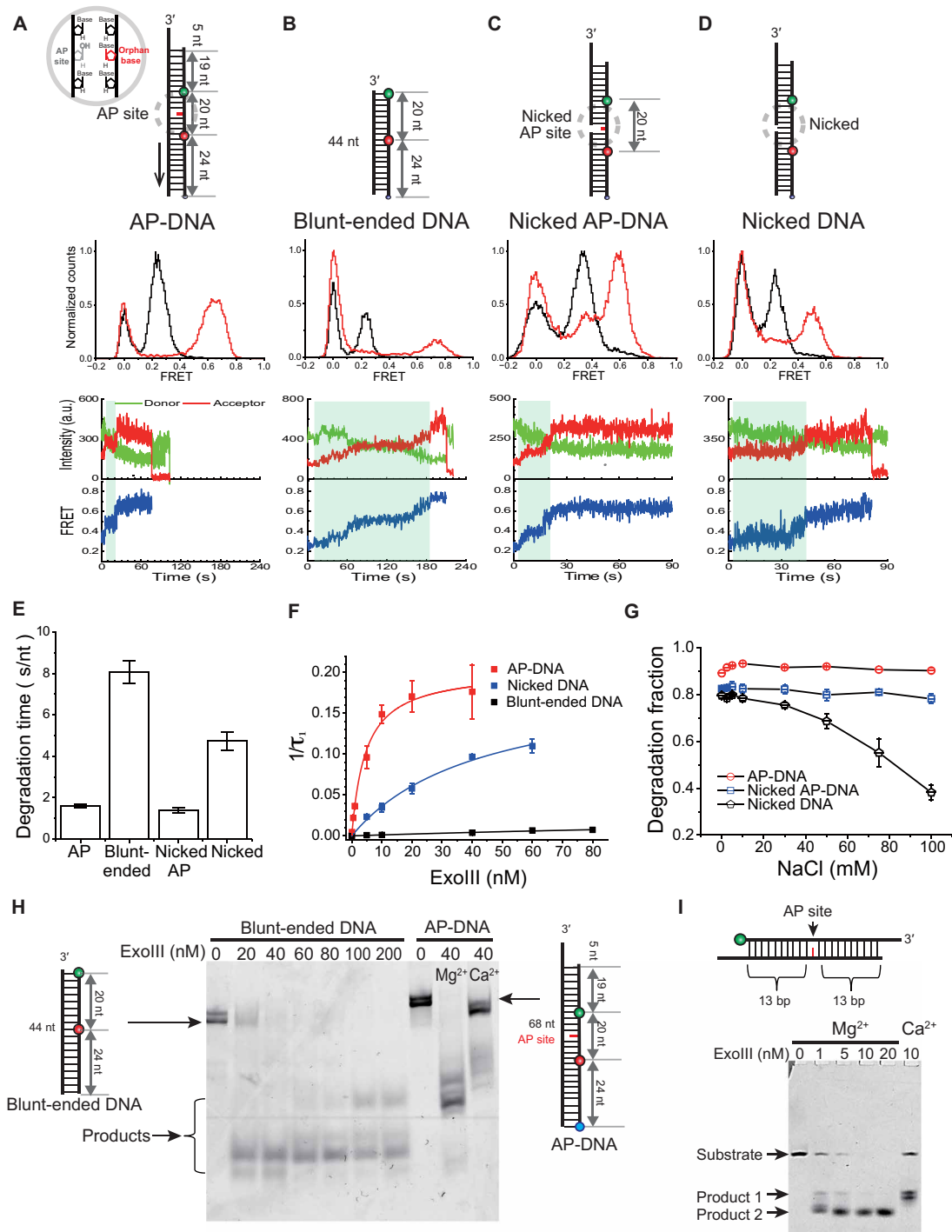


Fig. 2. In the presence of Mg²⁺, ExoIII processively degrades DNA substrates containing an AP site, whereas it performs distributive degradation on dsDNA substrates lacking an AP site (fig. S2). (A to D) Schematics of different substrates (top), smFRET histograms [middle, before (black) and after (red) reaction], and a representative FRET time trajectory (bottom) for different substrates. ExoIII (5 nM) and Mg²⁺ (10 mM) were added for the degradation reaction. (E) Average degradation time per nucleotide for various DNA substrates with SEM. Degradation times were determined during which FRET increases from the minimum to the maximum values. (F) Fraction degraded versus ExoIII concentration and single-exponential growth fits (fig. S5) for the three different substrates (AP-DNA, nicked DNA, and blunt-ended DNA), demonstrating ExoIII's strong affinity for the AP site. The tau (τ_1) is a characteristic time (fig. S5). (G) Fraction degraded versus NaCl concentration for the three different substrates (AP-DNA, nicked AP-DNA, and nicked DNA), showing a strong ExoIII affinity for the AP site even at high NaCl concentrations. (H) A gel-based degradation assay for blunt-ended DNA used for the single-molecule experiments in Fig. 1 and this figure. (I) In the presence of Mg²⁺, the enzyme nicks by its endonuclease activity and subsequently degrades downstream of the DNA substrate by its exonuclease activity (lanes 2 to 5). Product 1 is a fragment produced by AP endonucleolytic cleavage at the AP site, whereas product 2 is the final product by exonucleolytic degradation after cleavage at the AP site. In the presence of Ca²⁺ (lane 6), the enzyme cleaves at the AP site without significant further degradation.

from differences in the binding affinity for different substrates, the degradation activity was challenged by increasing NaCl to high-salt conditions in a wide range from 0 to 100 mM NaCl. The DNA substrates with an AP site (i.e., AP-DNA and nicked AP-DNA) showed robust degradation regardless of salt concentration, whereas nicked DNA lacking the AP site displayed a strong salt-dependent inhibition of degradation, with the lowest activity at 100 mM NaCl (Fig. 2G).

Overall, our findings demonstrate that the enzyme efficiently digests AP-containing substrates even at higher [NaCl] but less efficiently digests AP-lacking nicked DNA in a distributive manner, confirming that ExoIII binds tightly to the AP site (Fig. 2G). Both the faster degradation (Fig. 2, A to F) and the robust affinity (Fig. 2G) in the presence of AP sites imply that strong AP site recognition allows the enzyme to processively degrade a series of nucleotides without dissociation. The subtle difference in degradation activity between AP-DNA and nicked AP-DNA may indicate that the enzyme recognizes the backbone-intact AP site more readily than the backbone-nicked AP site (compare blue and red in Fig. 2G, which can be explained by the difference in affinities of Fig. 4F).

To investigate the role of protein association with the AP site, we performed a “single-turnover reaction,” in which the DNA substrate was incubated with ExoIII (~20 nM) in the absence of Mg^{2+} for ~2 min, allowing the enzyme to bind, and the reaction was initiated by introducing a flow of 10 mM Mg^{2+} without ExoIII. The flow also flushed out free proteins in solution; thus, only prebound ExoIII contributes to the reaction, allowing us to estimate how many nucleotides of DNA are degraded per single binding event (i.e., processivity). AP-DNA and nicked AP-DNA had significant degradation peaks at $E = 0.53$, suggesting that the enzyme firmly binds the AP site and processively degrades AP-containing substrates even in the Mg^{2+} flow (left panels in Fig. 3A and fig. S6). In contrast, nicked DNA and blunt-ended DNA without AP sites were not significantly degraded by the single-turnover reaction (right panels in Fig. 3A and fig. S6), since the Mg^{2+} flow removed the free proteins dissociating from the substrate by the distributive mode of action. This eventually terminated the reaction before complete degradation, clearly indicating that the enzyme performs distributive degradation in the absence of AP sites. These data from the AP site confirm that the enzyme is strongly constrained to the AP site during degradation by its tight binding and processively degrades the substrate.

Next, we carried out 2-min single-turnover reactions in various NaCl concentrations ranging from 0 to 100 mM to measure the processivity of how many nucleotides in AP-DNA could be degraded by ExoIII (Fig. 3B). Degradation trends changed at approximately 10 mM NaCl. Below that threshold, the exonuclease activity increased with [NaCl], but above the threshold, it decreased (Fig. 3, B and D), in contrast to the typical tendency of salt titration in which exonuclease activity gradually decreases with increasing salt concentrations because of unfavorable protein binding and high duplex stability (31–33). The different final FRET values indicated that the gap size generated depends on the salt concentration. To determine the gap size as a function of salt concentration, we constructed a calibration curve by measuring the FRET efficiency of different gap sizes, from 0 to 10 nt, in various NaCl concentrations (Fig. 3C) and found that the gap size varies from ~5 to 9 nt at concentrations below 10 mM NaCl but decreases to ~3 nt at 100 mM NaCl (Fig. 3D).

We examined whether the increase in FRET after the reaction resulted from bending of the DNA, rather than a processive and

sequential degradation, because a higher FRET could occur if the two dyes on the DNA substrate are brought closer by DNA bending upon protein binding, as reported in human ExoI (34) and FEN1 (35). Thus, we measured the relative distance between ExoIII and its substrate by labeling the protein at the N terminus with a donor (Cy3) by sortase (Fig. 4A and fig. S7) (36) and the AP-DNA substrate ~10 nt away from the AP site with an acceptor (Cy5) (Fig. 4B). After the Cy3-labeled mutant (D151N) was added to the Cy5-labeled AP-DNA, the binding and dissociation events of the fluorescently labeled protein were monitored without cleavage (Fig. 4C), displaying a FRET peak at $E = \sim 0.36$ (Fig. 4D). This distinct peak suggested that ExoIII specifically recognizes the AP site of the DNA substrate.

To estimate the FRET progression during the degradation process, we measured a FRET change using a series of DNA substrates that mimic the DNA degradation intermediates that could be generated as the degradation progresses. This measurement resulted in a gradual increase in FRET as the gap size increased owing to a decrease in the distance between the two dyes of the DNA and the protein (Fig. 4E). The gradual degradation of the AP-DNA might alter the affinity of ExoIII to degradation intermediates since the distance between the AP site being recognized and the 3' end being degraded increases as the degradation proceeds. We thus calculated the K_d values of various DNA substrates with and without the AP site, including their degradation intermediates based on binding and dissociation times (28, 37), and found that the affinity was high at the AP site. The K_d value of AP-DNA was ~50 times higher than that of no-AP-DNA (nicked DNA, blue bar at 0G in Fig. 4F), with K_d values of ~7 and ~350 nM, respectively (Fig. 4F). Upon the creation of a nick at the AP site, the affinity (K_d) decreased more than sevenfold from 7 to 52 nM at the 1-nt gap and became stabilized at approximately 9 nM for gap sizes larger than 4 nt (Fig. 4F). The affinity values (e.g., for AP-DNA, nicked AP-DNA, and nicked DNA) were in good agreement with the results of our bulk gel binding assays (fig. S8) and similar to those of human homolog APE1 (38).

We hypothesized that the high affinity at the AP site allowed the enzyme to remain bound at the AP site and to processively degrade the AP-DNA. To directly test this hypothesis using wild-type (WT) but Cy3-labeled ExoIII, we monitored the degradation reaction by FRET between Cy3-labeled WT ExoIII and Cy5-labeled AP-DNA in the presence of Mg^{2+} during gap creation. The FRET evolution of time traces (Fig. 5A) did not show any disappearance of the Cy3 signal until the FRET reached the maximum value and was consistent with the degradation mimic tendency with parabolic FRET growth (Fig. 4E), indicating that gradual exonucleolytic degradation took place while FRET increased. If the Cy3-labeled WT ExoIII were not processive and dissociated quickly, we would have observed dissociation events as abrupt disappearance of the Cy3 signal before FRET reached the maximum value. The final FRET, degradation, and binding times were ~0.74, ~0.88s, and ~3.37s, respectively (Fig. 5, B to D). This strongly suggested that the gap creation is processive in the presence of AP sites. In addition, the following facts also suggested that there is no significant bending: (i) The FRET value of the nicked AP-DNA itself without the addition of the protein is the same as the value of the AP-DNA after the AP endonuclease cleavage by Ca^{2+} (fig. S9), and (ii) a series of control experiments, including a high-salt dissociation assay (fig. S10) and a hybridization assay (figs. S11 and S12), confirmed that the FRET increase truly resulted from gap creation via sequential degradation, not from the bending of AP-DNA.

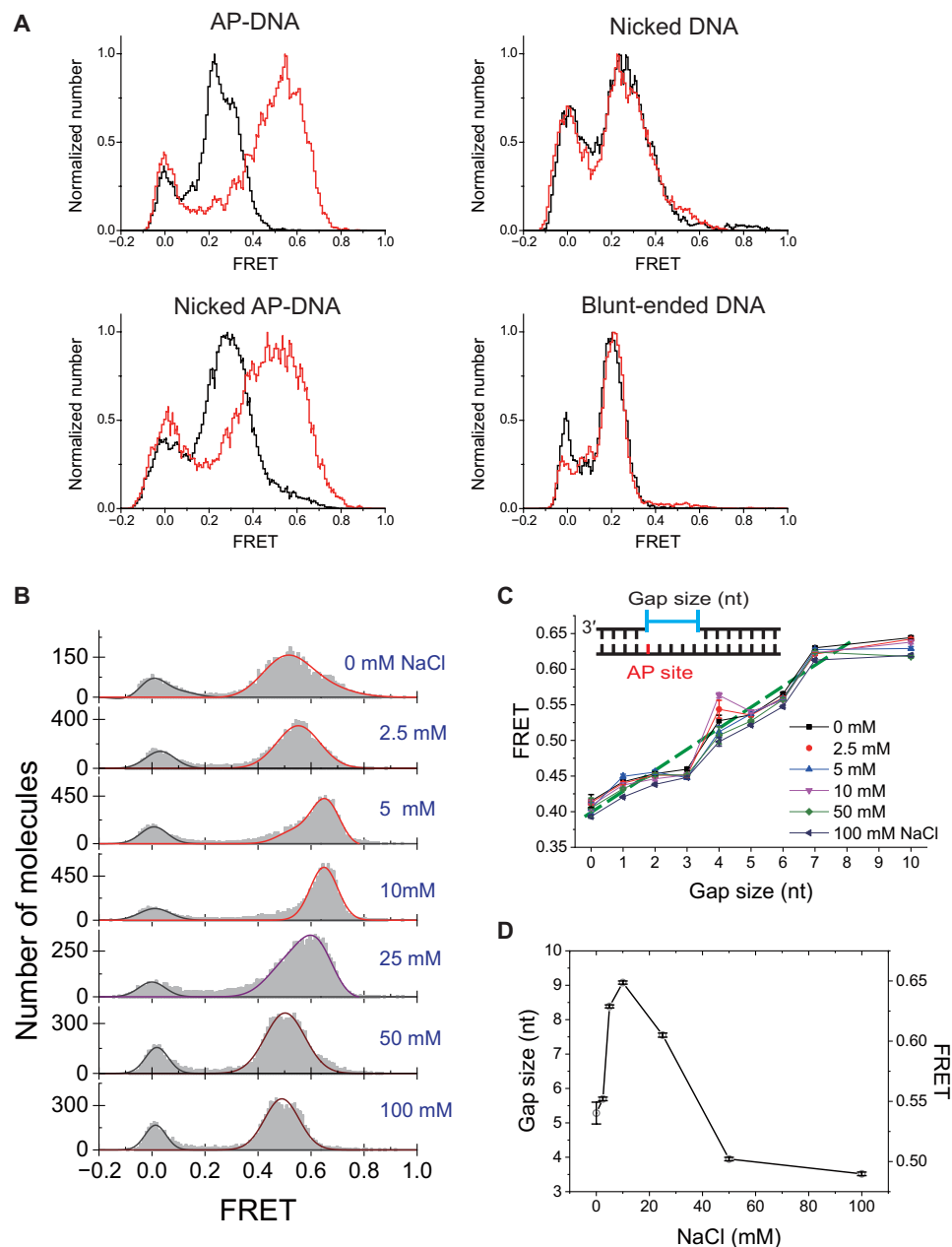


Fig. 3. ExoIII processively degrades the downstream DNA from the AP site without dissociating, and its degree of degradation strongly depends on salt concentration. (A) Single-turnover degradation reactions, in which no degradation is caused by free proteins rebinding from the solution, using various substrates. During the reaction, free proteins were not present, only bound proteins contributed to the reaction, and the reaction stopped if the bound proteins dissociated from the DNA. This reaction allows us to measure how many nucleotides the enzyme degrades per binding (fig. S6). (B) Single-turnover degradation reactions at various NaCl concentrations. Experiments were performed in the presence of 20 nM ExoIII unless otherwise mentioned. (C) Calibration curve of FRET efficiency and gap size measured at various salt concentrations with 10 mM Mg^{2+} . (D) FRET values were determined by fitting degradation FRET peaks at various NaCl concentrations, as presented in (B), and the gap size was interpolated from the FRET versus gap size curve of (C).

Gap processing might be influenced by the presence of polymerase I (pol I) during BER, but it is unknown how the two enzymes are temporally coordinated. To monitor gap processing by ExoIII and gap filling by pol I consecutively, we performed experiments in which equal amounts of ExoIII and pol I (1 nM each) were injected into a solution of AP-DNA in a buffer containing Mg^{2+} and deoxynucleoside triphosphates (dNTPs). More than ~52% ($n = 145$) of all traces displayed a unique pattern: an increase in FRET followed

by a decrease in FRET and a sharp increase in fluorescence between them (Fig. 6A, arrow). We attributed the FRET increase to degradation by ExoIII (orange region), the fluorescence jump to the binding of pol I (violet region), and the FRET decrease to the polymerization activity of pol I (green region).

To confirm our interpretation, we divided the experiment into two reactions. ExoIII was first preincubated with DNA in a buffer without Mg^{2+} for 2 min; then, pol I and Mg^{2+} in the absence of

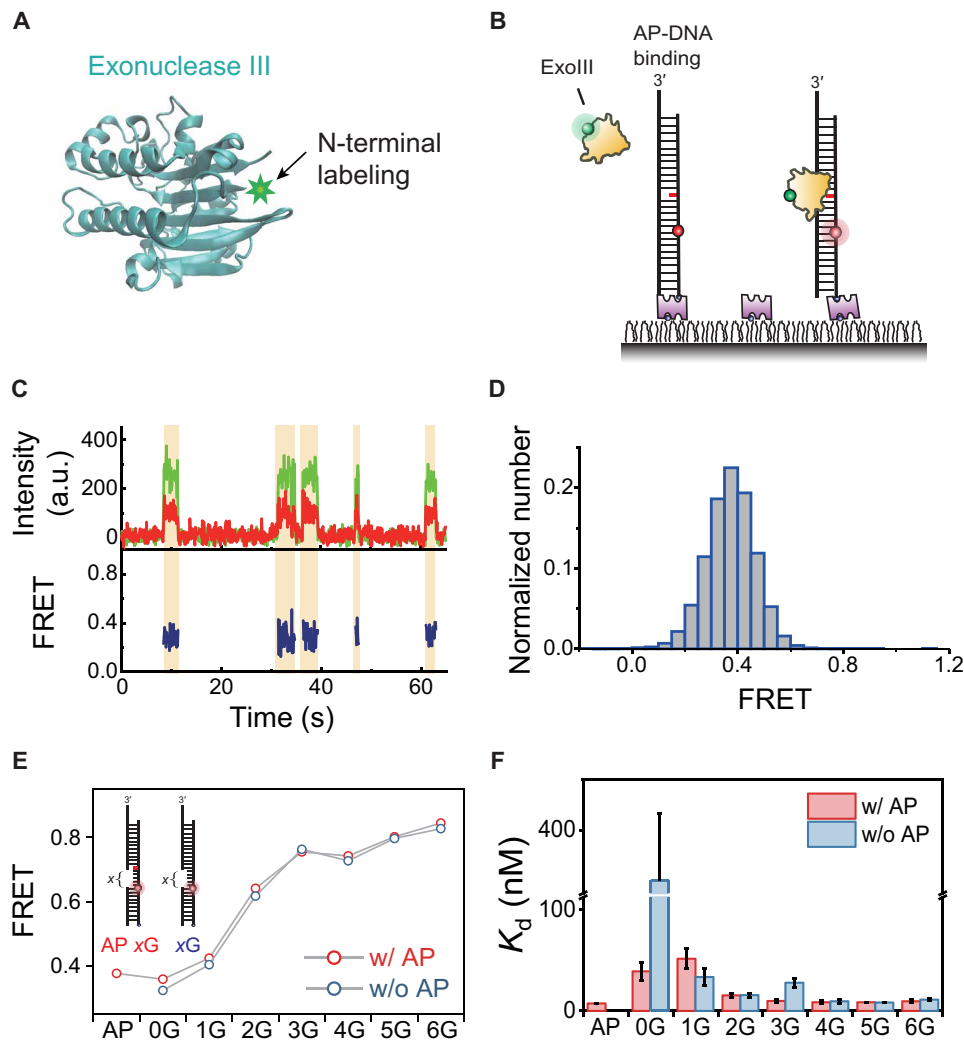


Fig. 4. Single-molecule protein imaging shows that the AP site provides a strong affinity to the DNA substrate and that there is no significant bending of DNA after AP-endonucleolytic cleavage. (A) A catalytic mutant of ExoIII (D151N) is labeled with a Cy3 fluorophore (green star) at the N terminus via site-specific labeling by sortase. (B) Experimental setup for monitoring direct protein binding, where Cy3-labeled ExoIII was added to a Cy5-labeled AP-DNA substrate immobilized on a fluorescence imaging surface. (C) A representative trace exhibiting distinct recognition of the AP site. (D) FRET histogram obtained from binding events to the AP site of DNA. (E) FRET evolutionary tendency calibrated as a function of gap size generated during gap processing (x stands for the gap size in number of nucleotides). (F) Progress in binding affinity (dissociation constant, K_d) as a function of gap size during gap creation. K_d is calculated as $K_d = k_{off}/k_{on}$, where k_{off} and k_{on} are obtained from single-exponential decay fitting on the distributions of binding and dissociation times.

dNTPs were added to trigger degradation but not to permit gap filling. This step allowed ExoIII to process the gap and pol I to load onto DNA when the gap became large enough. In the second reaction, proteins in solution were flushed out by a buffer containing Mg^{2+} and dNTPs. Thus, pol I would initiate gap filling only if it had preloaded during the previous degradation reaction. The first reaction involved robust gap processing, as evidenced by increased FRET efficiency even in the presence of pol I (Fig. 6B). In contrast, the second reaction revealed a dNTP-dependent FRET efficiency decrease, which was consistent with our interpretation (Fig. 6C).

To characterize this coordinated action, we measured the dwell times of the FRET increase and decrease as a function of dNTP concentration. The degradation rate obtained from the FRET increase was ~ 11.8 nt/s, whereas the polymerization rate obtained from the FRET decrease varied and fit Michaelis-Menten kinetics with a K_m

value of ~ 531 nM and a maximum velocity of ~ 12.5 nt/s, which was consistent with previous data (Fig. 6D) (39). The histogram obtained from the degradation (~ 443 molecules) revealed a FRET peak shift from ~ 0.36 to ~ 0.54 , corresponding to an average gap of ~ 5 nt, based on the calibration curve (Fig. 3C). The FRET value was very similar to that measured using ExoIII alone ($E = 0.53$). This suggests that when ExoIII first releases the 3' end, pol I quickly binds and synthesizes DNA from it. To confirm this, equal amounts of ExoIII and pol I in a buffer containing Mg^{2+} and dNTPs were mixed with a 10-nt 5' overhang duplex (mimicking the 3' side at the primer-template junction for polymerization). In this DNA construct, both enzymes competed for binding. The histogram of FRET shifted from a peak at ~ 0.46 before the reaction to a peak at ~ 0.22 after the reaction (fig. S13), suggesting that pol I has a higher binding affinity than ExoIII to the 3' end of the gap away from the AP

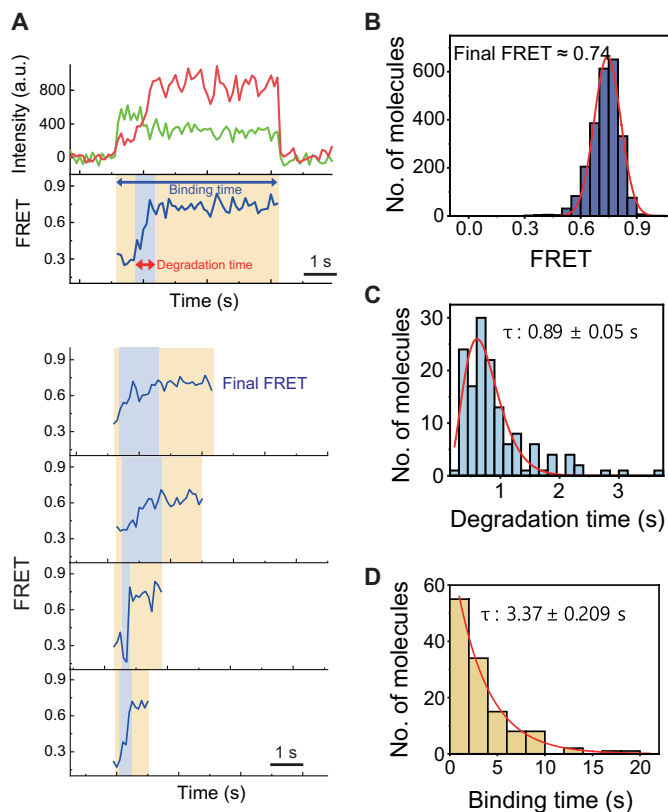


Fig. 5. Processive degradation in the presence of Mg^{2+} , directly monitored by Cy3-labeled WT ExoIII and Cy5-labeled AP-DNA. (A) Representative fluorescence intensity (top, green for donor and red for acceptor) and FRET efficiency (second and below) time trajectories show a gradual FRET increase during gap creation. (B) Histogram obtained from the final FRET values. (C) Histogram of total degradation times. (D) Histogram of binding times.

site and initiates DNA synthesis for repair. During gap creation, the high affinity of ExoIII to the AP site serves as the “intrinsic counting” mechanism that precisely counts and controls the size of the gap during BER.

DISCUSSION

The crystal structure of ExoIII [Protein Data Bank (PDB): 1AKO] and the cocrystal structure of human-homolog APE1 with AP site-containing DNA (PDB: 1DE8) are currently available (22, 40). The crystal structures and a biochemical study (23) suggested that both AP endonucleases specifically recognize the AP site. To understand this molecular mechanism, we reconstituted the DNA-enzyme complex *in silico*. The 71 conserved residues between ExoIII (22) and APE1 (40) were spatially superimposed on each other, and the other residues were aligned with respect to them using the VMD program (fig. S14). This *in silico* reconstitution elucidated how the enzyme achieves its strong affinity. First, a tryptophan (Trp^{212}) indole ring from ExoIII stacks on the nucleotide sugar ring at the AP site through a hydrophobic interaction (red ring group in Fig. 7A), providing strong affinity at the AP site (Figs. 2, F and G, and 4F). Second, the α_M helix (blue in Fig. 7A) clutches the 3' side of the undamaged DNA backbone via the major groove (22).

The reconstituted structure further revealed how the enzyme cleaves (endonuclease function) and digests (exonuclease function) the downstream DNA through a series of hydrolysis reactions (Fig. 7, B and C). First, the metal ions near Glu^{34} coordinate the phosphate group and polarize the P—O3' bond, which induces a kink at the P—O3' bond (Fig. 7B, red circle). This overall effect, along with the ring-stacking interaction at the AP site and the electrostatic interaction at the charged surface, achieves a transition state that allows the cleavage reaction (22). Second, the catalytic triad-like Asp-His- H_2O bridge acts as a proton acceptor and donor, thus initiating a single metal ion-aided nucleophilic attack on the P—O3' bond at Glu^{34} in the active site (Fig. 7B, green) (22). Last, two charged residues (Lys^{121} and Asn^{153} in Fig. 7C) along the downstream attract phosphates for successive cleavage reactions. This attraction-based model is analogous to the mechanism proposed for a processive λ exonuclease (41).

By combining our observations of tight binding to the AP site (Fig. 4F), processive degradation without dissociation (Figs. 3A and 5A), structural reconstitution of AP site recognition, and the attraction-based model for exonuclease activity (Fig. 7, A and B), we propose the following mechanism. ExoIII, belonging to the type II family of AP endonucleases, specifically cuts 5' to the AP site and then consecutively digests DNA in the 3'-to-5' direction using its exonucleolytic activity while anchored at the AP site (Fig. 7D). During degradation, the AP site (Fig. 7D, pink oval) functions as a binding hotspot. The strong affinity to the AP site allows the enzyme to tightly bind the substrate and processively digest the damaged strand downstream without dissociation. However, the physical constraint at the AP site limits how far the enzyme can degrade and determine the gap size. The enzyme digests until its exonucleolytic pulling and the rigidity of ssDNA or electrostatic interaction between the protein and its substrate are balanced. During degradation, there is an intermediate ssDNA loop, created by the enzyme pulling in the other strand while anchored at the AP site (Fig. 7D, top right), a process that is reminiscent of the prime loop observed in the T7 replisome (42, 43). Mutagenesis studies by electrophoretic mobility shift assay confirmed that mutations at the aromatic rings (i.e., W212A, W212S, and W212A/F213A) significantly reduced enzymatic binding affinity to the AP-DNA (fig. S15).

We attribute the difference in rates to whether the degradation reaction is processive or distributive, but one could argue that the enzyme is more catalytically efficient because of the presence of an AP site so dissociation and reassociation may not be the cause. Although the AP site processing time was too short to accurately measure the difference in cleavage rate, the following data suggested that the difference in rate presumably originated from the difference in binding and dissociation. The difference in K_d between DNA substrates with and without an AP site was ~ 50 times (Fig. 4F), and FRET time trajectories obtained from Cy3-labeled WT ExoIII and Cy5-labeled AP-DNA directly showed processive degradation without detectable marked pauses and without disappearance of the fluorescent signal (Fig. 5). In addition, traditional experiments (44, 45) with a DNA trap for enzymatic processivity revealed that ExoIII performs processive degradation on the AP-DNA but performs distributive degradation on the blunt-ended DNA in the presence of a DNA trap (fig. S16).

The tendency of the biphasic degradation shown in Fig. 3D could be explained by our proposed mechanism. Under low-salt conditions, the negative-charge repulsion of phosphate groups in

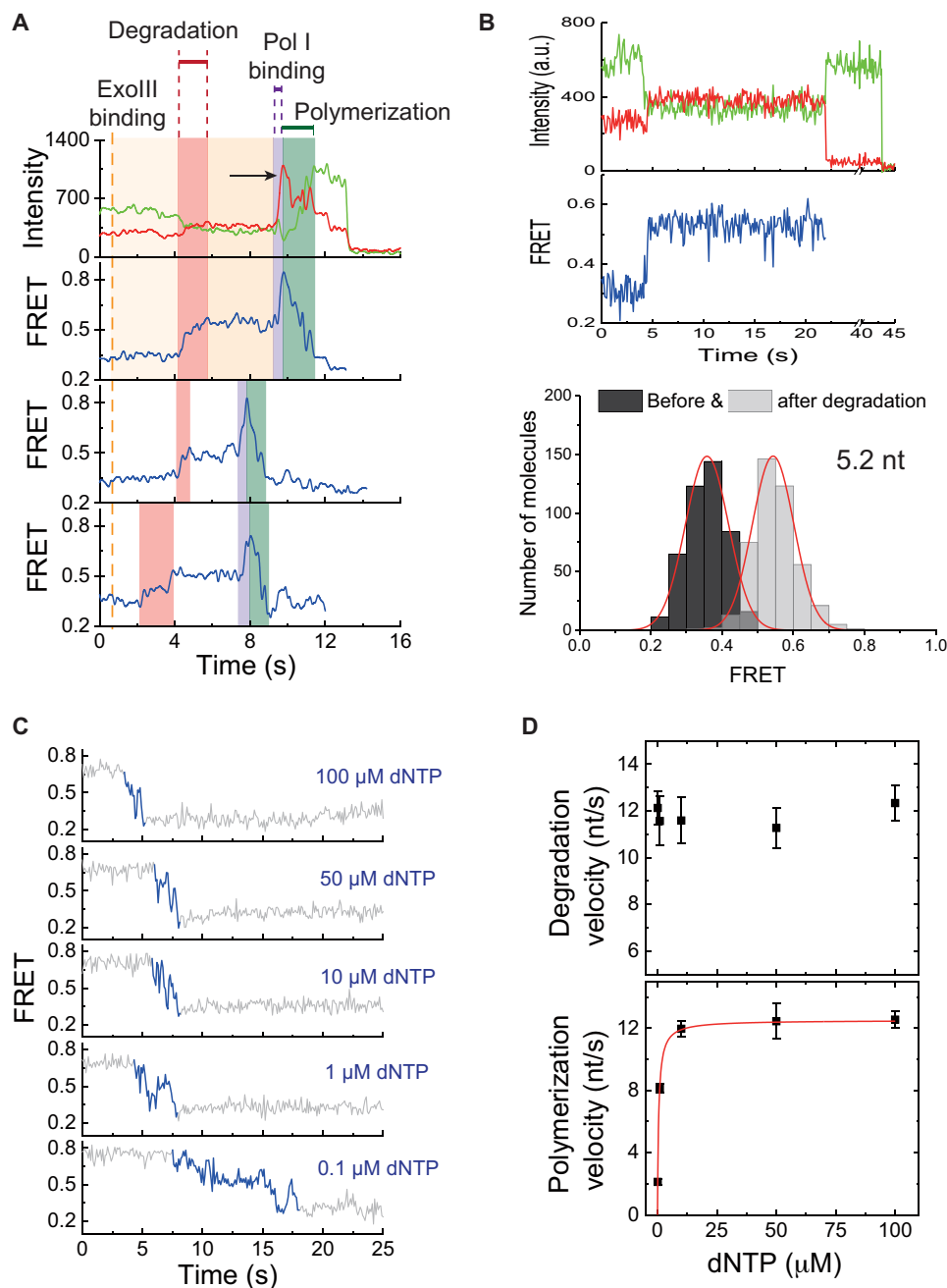


Fig. 6. Coordinated gap processing and gap filling by ExoIII and pol I. (A) Representative fluorescence intensity (top, green for donor and red for acceptor) and FRET efficiency time trajectories (blue) with the characteristic features of degradation (orange region), polymerase binding (violet region), and polymerization (green region). The experiments were performed by adding ExoIII and pol I to AP-DNA in a solution containing Mg^{2+} and dNTPs. (B) Representative FRET time trajectory (top two panels) and histograms (bottom) before (black) and after (gray) degradation. The FRET efficiency shift caused by degradation in the presence of pol I indicates that the gap size is approximately 5 to 6 nt long. (C) Representative smFRET time trajectories taken from polymerization reactions with various dNTP concentrations after the degradation reaction performed in (B). (D) Degradation rate and polymerization rate as a function of dNTP concentration. The degradation rate does not change, whereas the polymerization rate is strongly dependent on the dNTP concentration. The polymerization rate follows Michaelis-Menten kinetics with a maximum velocity of ~ 12.5 nt/s and a K_m value of ~ 513 nM dNTP. How reaction rates are calculated is described in the Supplementary Materials.

the ssDNA loop provides resistance during degradation, but under high-salt conditions, the duplex is stabilized (46). Thus, degradation becomes favorable because the resulting intermediate loop becomes flexible (47, 48), whereas degradation is more demanding under high-salt conditions because the dsDNA is more stable (49).

A similar decreasing trend in exonuclease activity was reported as a function of salt concentration (12). If ExoIII degraded the DNA strand without anchoring at 5' to the AP site (Fig. 7D, bottom right), this behavior would not be observed under low-salt conditions. For this reason, the gap size is biphasically influenced by salt

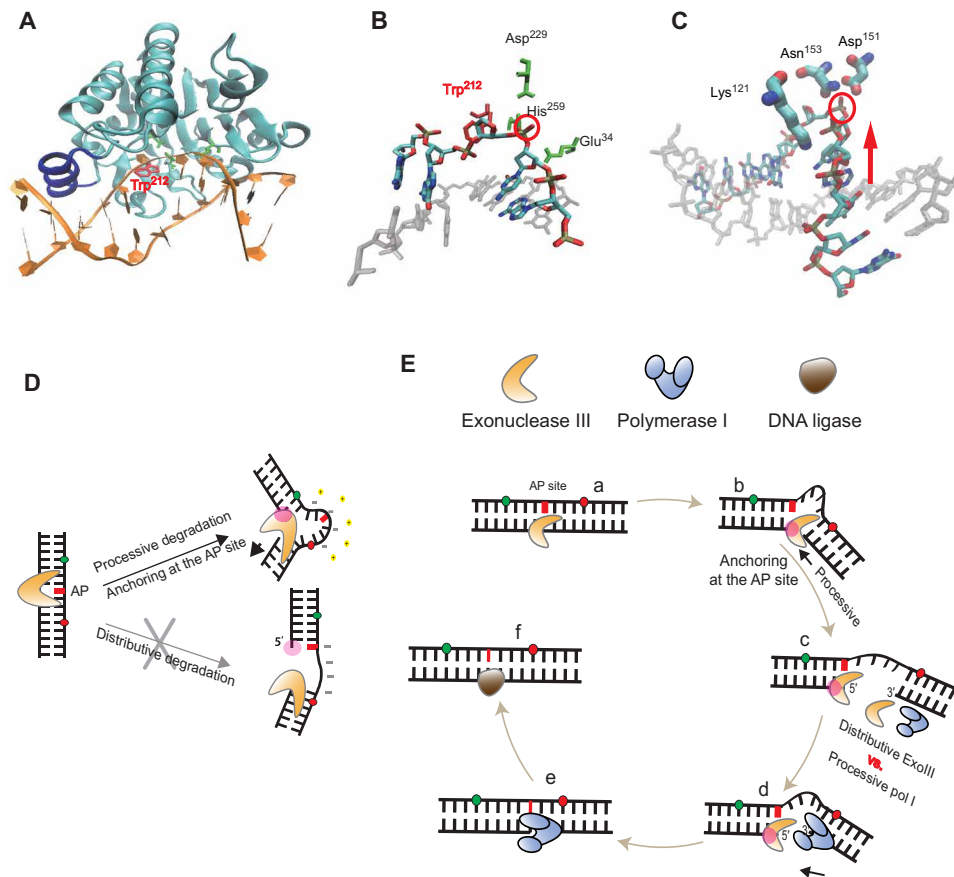


Fig. 7. Model of AP site-specific anchoring mechanism. (A) In silico model of ExoIII and a DNA complex showing AP site-specific binding, in which the tryptophan (Trp²¹²) indole ring stacks on the nucleotide sugar ring at the AP site (red) (fig. S14C). (B) The catalytic residues (green) and the coordination of the phosphate group by a metal ion induce a kink at the P–O3' bond (red circle), inducing a nucleophilic attack on the P–O3' bond during the enzymatic cleavage reaction. (C) Molecular basis of exonuclease activity. Two charged residues (Lys¹²¹ and Asn¹⁵³) around the active site provide an attraction force to pull in the negatively charged phosphates along the hydrolyzable strand for a successive cleavage reaction. (D) ExoIII tightly anchors itself to the AP site, cleaves 5' to the AP site, and processively digests DNA in the 3'-to-5' direction without dissociating. The physical constraint of being at the AP site limits the gap size. (E) Model of BER. (a) ExoIII binds to the AP site via the tryptophan (Trp²¹²) indole ring. (b) The exonuclease anchors itself at the AP site, cleaves at the AP site, and processively digests the downstream DNA, yielding an intermediate ssDNA loop during degradation. The physical constraint of the enzyme to bind at the AP site limits the size of the gap created, and the ssDNA loop may confer resistance against enzyme activity. (c and d) Upon the first release of the 3' end from ExoIII, pol I and ExoIII compete to occupy the 3' end, but pol I eventually wins because of the nature of ExoIII's distributive exonuclease activity. Thus, ExoIII achieves processive degradation from the AP site, whereas it performs distributive degradation at the 3' side of the gap. (e) Pol I fills the gap upon loading the 3' end and removes the AP site through its 5' dRP lyase activity. (f) DNA ligase seals the nick.

concentration, which affects not only the rigidity of the loop but also the duplex stability of DNA. In the low-salt condition, the loop is the main gap-controlling factor, acting as a resisting modulator, but in the high-salt condition, the duplex stability becomes the key determinant.

The mechanism of gap creation relies on binding affinity. The 5' side of the gap is a strong binding site for ExoIII because of the AP site, whereas the 3' side is a target for both ExoIII and pol I (Fig. 7E-c). However, pol I can outcompete ExoIII (fig. S13). On the basis of the data, we propose a comprehensive model. ExoIII binds and creates a nick at the AP site using an AP-specific endonuclease (Fig. 7E-a); at the 5' side, ExoIII processively degrades the downstream DNA in the 3'-to-5' direction while tightly anchored to the AP site (Fig. 7E-b). Both ExoIII and pol I compete for the 3' end, which is liberated from the physically constrained ExoIII (Fig. 7E-c). Pol I ultimately wins in binding to the 3' end liberated away from the AP site due to the nature of ExoIII's distributive degradation activity on the 3' end

distant from the AP site (Fig. 7E-d and fig. S13). Pol I synthesizes DNA from the 3' end of the gap (Fig. 7E-e), removes the AP site using its 5'-dRP lyase activity, and ligases the nick (Fig. 7E-f).

Exposure of ssDNA leads to damage or breaks from a myriad of chemical and enzymatic attacks. The significance of protecting ssDNA from damage can be emphasized by the evolutionary conservation of single-stranded binding protein (SSB) across all species. SSB generally protects the ssDNA produced during replication and DNA repair processes. However, SSB cannot securely bind and protect DNA shorter than 35 nt because of its intrinsic required binding length (24) and the ssDNA gap cannot be therefore protected by SSB. For this reason, quick processing and restriction of the gap size are very important for genomic stability during BER. To efficiently orchestrate the process, evolution must optimize the anchor-based molecular mechanism that controls thermodynamics and kinetics to catalyze the whole process in a timely manner. Because of the built-in mechanism, the gap size is strictly regulated to be

long enough to recruit DNA polymerase during BER but short enough to protect its single-stranded portion against ssDNA-specific nucleases.

To date, many aspects of how a series of steps in BER are coordinated during BER have not been well understood because of the lack of dynamic information. Our study has provided new insights into the fundamental mechanism of ExoIII with respect to its endonuclease and exonuclease activities and its coordination with pol I during gap creation, which primes BER. We also demonstrate the enzymatic conversion, in which ExoIII transforms its intrinsic distributive activity to de novo processive activity in response to DNA damage (i.e., the AP site) to limit the gap size to maintain genomic stability. ExoIII at the AP site pulls DNA for degradation, which is reminiscent of the reeling mechanism of PcrA helicase, which sits on a junction and pulls in the downstream DNA to remove single-stranded binding proteins such as RecA and SSB (50).

MATERIALS AND METHODS

Protein and DNA preparation

WT ExoIII was purchased from New England Biolabs (NEB) (catalog #M0206S), and all mutants and fluorescently labeled WT ExoIII were purified (Supplementary Materials). DNA pol I was purchased from New England Biolabs (catalog #M0209S). All DNA oligonucleotides, including the AP site-containing strand, were purchased from Integrated DNA Technologies. Biotin was conjugated to the 3' end of 5' nonhydrolyzed strands. Each Cy3 and Cy5 (NHS-ester from GE Healthcare) were incorporated into two oligos of DNA strands via an internal modification (dT with a C6 amino linker). The oligos were annealed with the complementary strand and ligated in a duplex form by T4 DNA ligase (NEB; catalog #M0202S). Sequences of DNA and positions of biotin and fluorescent dyes are provided in the Supplementary Materials.

Single-molecule experiments

DNA constructs were immobilized on polyethylene glycol (PEG; Laysan Bio Inc.)-functionalized quartz surface to minimize non-specific protein binding onto the surface. Immobilization was held by neutravidin (Pierce) and biotin interaction at the ends of DNA and biotin-modified PEG on the surface. Approximately 10 to 50 pM concentrations of DNA constructs were injected into the imaging chamber to achieve an appropriate density for single-molecule imaging. An oxygen scavenger system with catalase, glucose oxidase, and D-glucose was used to prevent rapid photobleaching of fluorescent dyes. The reaction buffer contained 50 mM tris-HCl (pH 7.5), 10 mM MgCl₂, bovine serum albumin (50 µg/ml), 1 mM dithiothreitol, Trolox (1 mg/ml) (Sigma-Aldrich), and the oxygen scavenging system of glucose oxidase (1 mg/ml) (Sigma-Aldrich) and 0.4% (w/v) D-glucose (Sigma-Aldrich). A flow channel was constructed by assembling a coverslip onto a microscope slide using double-sided tape and sealing the edge of the slide with epoxy. A 1-ml syringe was connected to the outlet hole on the flow chamber through tubing, and a pipette tip reservoir containing a reaction solution was built on the inlet hole. When the syringe was pulled, the solution was delivered into the chamber at a rate of ~10 µl/s. The mult turnover reaction was started by introducing a buffer containing ExoIII and Mg²⁺ into DNA substrates tethered on the surface of an imaging chamber at room temperature. In contrast, the single-turnover reaction, where DNA substrates were preincubated with ExoIII for ~2 min in the absence of Mg²⁺, was started by flowing in Mg²⁺ buffer.

Data acquisition

A prism-type total internal reflection fluorescence microscope was used to acquire fluorescence emission signals from Cy3 and Cy5 by a water immersion objective lens (UPlanApo 60×, Olympus). The laser scattering was rejected through a 550-nm long-pass filter. The fluorescence emission light was further separated into donor and acceptor signals with a 630- or 635-nm dichroic mirror (Chroma) and projected onto a back-illuminated electron-multiplying charge-coupled device (Andor) with a time resolution of 30 to 100 ms. Fluorescence signals of the donor and acceptor were amplified by a gain before camera readout. Thus, both recorded fluorescence intensities of Cy3 and Cy5 are in an arbitrary unit (a.u.), proportional to their photon counts. FRET efficiency is determined by the ratio of intensities, $\text{Intensity}_{\text{acceptor}} / (\text{Intensity}_{\text{donor}} + \text{Intensity}_{\text{acceptor}})$ after correcting for cross-talk between the donor and acceptor channels. All data were analyzed by MATLAB codes and plotted in Origin.

SUPPLEMENTARY MATERIALS

Supplementary material for this article is available at <http://advances.sciencemag.org/cgi/content/full/7/29/eabg0076/DC1>

[View/request a protocol for this paper from Bio-protocol.](#)

REFERENCES AND NOTES

1. A. B. Robertson, A. Klungland, T. Rognes, I. Leiros, DNA repair in mammalian cells: Base excision repair: The long and short of it. *Cell. Mol. Life Sci.* **66**, 981–993 (2009).
2. S. van der Veen, C. M. Tang, The BER necessities: The repair of DNA damage in human-adapted bacterial pathogens. *Nat. Rev. Microbiol.* **13**, 83–94 (2015).
3. R. M. Kohli, Y. Zhang, TET enzymes, TDG and the dynamics of DNA demethylation. *Nature* **502**, 472–479 (2013).
4. R. C. Centore, R. Lestini, S. J. Sandler, XthA (Exonuclease III) regulates loading of RecA onto DNA substrates in log phase *Escherichia coli* cells. *Mol. Microbiol.* **67**, 88–101 (2008).
5. J. D. Levin, A. W. Johnson, B. Demple, Homogeneous *Escherichia coli* endonuclease IV. Characterization of an enzyme that recognizes oxidative damage in DNA. *J. Biol. Chem.* **263**, 8066–8071 (1988).
6. B. Weiss, L. Grossman, Phosphodiesterases involved in DNA repair. *Adv. Enzymol. Relat. Areas Mol. Biol.* **60**, 1–34 (1987).
7. S. G. Rogers, B. Weiss, Exonuclease III of *Escherichia coli* K-12, an AP endonuclease. *Methods Enzymol.* **65**, 201–211 (1980).
8. R. Roychoudhury, R. Wu, Novel properties of *Escherichia coli* exonuclease III. *J. Biol. Chem.* **252**, 4786–4789 (1977).
9. S. Henikoff, Unidirectional digestion with exonuclease III creates targeted breakpoints for DNA sequencing. *Gene* **28**, 351–359 (1984).
10. C. C. Richardson, I. R. Lehman, A. Kornberg, A deoxyribonucleic acid phosphatase-exonuclease from *Escherichia coli*: II. Characterization of the exonuclease activity. *J. Biol. Chem.* **239**, 251–258 (1964).
11. Y. Liu, R. Prasad, W. A. Beard, P. S. Kedar, E. W. Hou, D. D. Shock, S. H. Wilson, Coordination of steps in single-nucleotide base excision repair mediated by apurinic/aprimidinic endonuclease 1 and DNA polymerase β. *J. Biol. Chem.* **282**, 13532–13541 (2007).
12. G. Lee, M. A. Bratkowski, F. Ding, A. Ke, T. Ha, Elastic coupling between RNA degradation and unwinding by an exoribonuclease. *Science* **336**, 1726–1729 (2012).
13. G. Lee, J. Yoo, B. J. Leslie, T. Ha, Single-molecule analysis reveals three phases of DNA degradation by an exonuclease. *Nat. Chem. Biol.* **7**, 367–374 (2011).
14. S. Myong, M. M. Bruno, A. M. Pyle, T. Ha, Spring-loaded mechanism of DNA unwinding by hepatitis C virus NS3 helicase. *Science* **317**, 513–516 (2007).
15. E. A. Abbondanzieri, G. Bokinsky, J. W. Rausch, J. X. Zhang, S. F. J. Le Grice, X. Zhuang, Dynamic binding orientations direct activity of HIV reverse transcriptase. *Nature* **453**, 184–189 (2008).
16. T. D. Christian, L. J. Romano, D. Rueda, Single-molecule measurements of synthesis by DNA polymerase with base-pair resolution. *Proc. Natl. Acad. Sci. U.S.A.* **106**, 21109–21114 (2009).
17. A. M. van Oijen, P. C. Blainey, D. J. Crampton, C. C. Richardson, T. Ellenberger, X. S. Xie, Single-molecule kinetics of λ exonuclease reveal base dependence and dynamic disorder. *Science* **301**, 1235–1238 (2003).
18. S. Arslan, R. Khafizov, C. D. Thomas, Y. R. Chemla, T. Ha, Engineering of a superhelicase through conformational control. *Science* **348**, 344–347 (2015).
19. M. J. Comstock, K. D. Whitley, H. Jia, J. Sokoloski, T. M. Lohman, T. Ha, Y. R. Chemla, Direct observation of structure-function relationship in a nucleic acid-processing enzyme. *Science* **348**, 352–354 (2015).

20. S. Hohng, R. Zhou, M. K. Nahas, J. Yu, K. Schulten, D. M. J. Lilley, T. Ha, Fluorescence-force spectroscopy maps two-dimensional reaction landscape of the Holliday junction. *Science* **318**, 279–283 (2007).
21. M. T. Woodside, P. C. Anthony, W. M. Behnke-Parks, K. Larizadeh, D. Herschlag, S. M. Block, Direct measurement of the full, sequence-dependent folding landscape of a nucleic acid. *Science* **314**, 1001–1004 (2006).
22. C. D. Mol, C.-F. Kuo, M. M. Thayer, R. P. Cunningham, J. A. Tainer, Structure and function of the multifunctional DNA-repair enzyme exonuclease III. *Nature* **374**, 381–386 (1995).
23. K. Kaneda, J. Sekiguchi, T. Shida, Role of the tryptophan residue in the vicinity of the catalytic center of exonuclease III family AP endonucleases: AP site recognition mechanism. *Nucleic Acids Res.* **34**, 1552–1563 (2006).
24. R. Roy, S. Hohng, T. Ha, A practical guide to single-molecule FRET. *Nat. Methods* **5**, 507–516 (2008).
25. P. R. Selvin, T. Ha, *Single-Molecule Techniques: A Laboratory Manual* (Cold Spring Harbor Laboratory Press, ed. 1, 2008), vol. 1.
26. H. Hwang, H. Kim, S. Myong, Protein induced fluorescence enhancement as a single molecule assay with short distance sensitivity. *Proc. Natl. Acad. Sci. U.S.A.* **108**, 7414–7418 (2011).
27. N. K. Maluf, C. J. Fischer, T. M. Lohman, A dimer of *Escherichia coli* UvrD is the active form of the helicase in vitro. *J. Mol. Biol.* **325**, 913–935 (2003).
28. S. Myong, S. Cui, P. V. Cornish, A. Kirchhofer, M. U. Gack, J. U. Jung, K.-P. Hopfner, T. Ha, Cytosolic viral sensor RIG-I is a 5'-triphosphate-dependent translocase on double-stranded RNA. *Science* **323**, 1070–1074 (2009).
29. D. Brutlag, A. Kornberg, Enzymatic synthesis of deoxyribonucleic acid: XXXVI. A proofreading function for the 3' → 5' exonuclease activity in deoxyribonucleic acid polymerases. *J. Biol. Chem.* **247**, 241–248 (1972).
30. B. Luckow, R. Renkawitz, G. Schütz, A new method for constructing linker scanning mutants. *Nucleic Acids Res.* **15**, 417–429 (1987).
31. M. Takeuchi, R. Lillis, B. Demple, M. Takeshita, Interactions of *Escherichia coli* endonuclease IV and exonuclease III with abasic sites in DNA. *J. Biol. Chem.* **269**, 21907–21914 (1994).
32. L.-H. Guo, R. Wu, New rapid methods for DNA sequencing based on exonuclease III digestion followed by repair synthesis. *Nucleic Acids Res.* **10**, 2065–2084 (1982).
33. J. F. Tomb, G. J. Barcak, Regulating the 3'-5' activity of exonuclease III by varying the sodium chloride concentration. *Biotechniques* **7**, 932–933 (1989).
34. J. Orans, E. A. McSweeney, R. R. Iyer, M. A. Hast, H. W. Hellinga, P. Modrich, L. S. Beese, Structures of human exonuclease I DNA complexes suggest a unified mechanism for nuclease family. *Cell* **145**, 212–223 (2011).
35. S. E. Tsutakawa, S. Classen, B. R. Chapados, A. S. Arvai, L. D. Finger, G. Guenther, C. G. Tomlinson, P. Thompson, A. H. Sarker, B. Shen, P. K. Cooper, J. A. Grasyk, J. A. Tainer, Human flap endonuclease structures, DNA double-base flipping, and a unified understanding of the FEN1 superfamily. *Cell* **145**, 198–211 (2011).
36. C. S. Theille, M. D. Witte, A. E. M. Blom, L. Kundrat, H. L. Ploegh, C. P. Guimaraes, Site-specific N-terminal labeling of proteins using sortase-mediated reactions. *Nat. Protoc.* **8**, 1800–1807 (2013).
37. E. Marklund, B. van Oosten, G. Mao, E. Amselem, K. Kipper, A. Sabantsev, A. Emmerich, D. Globisch, X. Zheng, L. C. Lehmann, O. G. Berg, M. Johansson, J. Elf, S. Deindl, DNA surface exploration and operator bypassing during target search. *Nature* **583**, 858–861 (2020).
38. J. W. Hill, T. K. Hazra, T. Izumi, S. Mitra, Stimulation of human 8-oxoguanine-DNA glycosylase by AP-endonuclease: Potential coordination of the initial steps in base excision repair. *Nucleic Acids Res.* **29**, 430–438 (2001).
39. M. Camps, L. A. Loeb, When Pol I goes into high gear: Processive DNA synthesis by Pol I in the cell. *Cell Cycle* **3**, 116–118 (2004).
40. C. D. Mol, T. Izumi, S. Mitra, J. A. Talner, DNA-bound structures and mutants reveal abasic DNA binding by APE1 DNA repair and coordination. *Nature* **403**, 451–456 (2000).
41. J. Zhang, K. A. McCabe, C. E. Bella, Crystal structures of λ exonuclease in complex with DNA suggest an electrostatic ratchet mechanism for processivity. *Proc. Natl. Acad. Sci. U.S.A.* **108**, 11872–11877 (2011).
42. N. E. Dixon, DNA replication: Prime-time looping. *Nature* **462**, 854–855 (2009).
43. M. Pandey, S. Syed, I. Donmez, G. Patel, T. Ha, S. S. Patel, Coordinating DNA replication by means of priming loop and differential synthesis rate. *Nature* **462**, 940–943 (2009).
44. M. T. Washington, R. E. Johnson, S. Prakash, L. Prakash, Fidelity and processivity of *Saccharomyces cerevisiae* DNA polymerase η . *J. Biol. Chem.* **274**, 36835–36838 (1999).
45. J. Wu, A. de Paz, B. M. Zamft, A. H. Marblestone, E. S. Boyden, K. P. Kording, K. E. J. Tyo, DNA binding strength increases the processivity and activity of a Y-Family DNA polymerase. *Sci. Rep.* **7**, 4756 (2017).
46. S. B. Smith, Y. Cui, C. Bustamante, Overstretching B-DNA: The elastic response of individual double-stranded and single-stranded DNA molecules. *Science* **271**, 795–799 (1996).
47. S. B. Smith, L. Finzi, C. Bustamante, Direct mechanical measurements of the elasticity of single DNA molecules by using magnetic beads. *Science* **258**, 1122–1126 (1992).
48. A. Bosco, J. Camunas-Soler, F. Ritort, Elastic properties and secondary structure formation of single-stranded DNA at monovalent and divalent salt conditions. *Nucleic Acids Res.* **42**, 2064–2074 (2013).
49. H. Clausen-Schaumann, M. Rief, C. Tolksdorf, H. E. Gaub, Mechanical stability of single DNA molecules. *Biophys. J.* **78**, 1997–2007 (2000).
50. J. Park, S. Myong, A. Niedziela-Majka, K. S. Lee, J. Yu, T. M. Lohman, T. Ha, PcrA helicase dismantles RecA filaments by reeling in DNA in uniform steps. *Cell* **142**, 544–555 (2010).

Acknowledgments: We thank T. Shida for the gift of plasmids and C. Joo, J.-B. Lee, and K. Lee for helpful discussion. **Funding:** This work was supported by the GIST Research Institute (GRI) in 2021 and the National Research Foundation of Korea (NRF) grant funded by the Korean government (NRF-2020R1A2C2006712 and NRF-2019R1A4A1028802) and by a grant from the Korean Health Technology R&D Project, Ministry of Health and Welfare, Republic of Korea (HA17C0031: #1720050). **Author contributions:** G.L. conceived the project. J.Y., D.L., H.I., S.J., and S.O. performed the experiments and analyzed the data, and M.S. and D.P. provided experimental insight and interpretation. J.Y., D.L., and G.L. wrote the manuscript with input from all authors. **Competing interests:** The authors declare that they have no competing interests. **Data and materials availability:** All data needed to evaluate the conclusions in the paper are present in the paper and/or the Supplementary Materials. Additional data related to this paper may be requested from the authors.

Submitted 4 December 2020

Accepted 28 May 2021

Published 14 July 2021

10.1126/sciadv.abg0076

Citation: J. Yoo, D. Lee, H. Im, S. Ji, S. Oh, M. Shin, D. Park, G. Lee, The mechanism of gap creation by a multifunctional nuclease during base excision repair. *Sci. Adv.* **7**, eabg0076 (2021).